Inorganic Chemistry

ARTICLE

pubs.acs.org/IC

Spectroscopic and Electronic Structure Studies Probing Covalency Contributions to C−H Bond Activation and Transition-State Stabilization in Xanthine Oxidase

Joseph Sempombe, Benjamin Stein, and Martin L. Kirk*

Department of Chemistry and Chemical Biology, The University of New Mexico, MSC03 2060, 1 University of New Mexico, Albuquerque, New Mexico 87131-0001, United States

ABSTRACT: A detailed electron paramagnetic resonance (EPR) and computational study of a key paramagnetic form of xanthine oxidase (XO) has been performed and serves as a basis for developing a valence-bond description of C−H activation and transition-state (TS) stabilization along the reaction coordinate with aldehyde substrates. EPR spectra of aldehyde-inhibited XO have been analyzed in order to provide information regarding the relationship between the **g**, ^{95,97}Mo hyperfine ($\mathbf{A}^{Mo}$), and ^{13}C hyperfine ($\mathbf{A}^{C}$) tensors. Analysis of the EPR spectra has allowed for greater insight into the electronic origin of key delocalizations within the Mo−O_{eq}−C fragment and how these contribute to C−H bond activation/cleavage and TS stabilization. A natural bond orbital analysis of the enzyme reaction coordinate with aldehyde substrates shows that both Mo═S $\pi \rightarrow$ C−H σ^* (ΔE = 24.3 kcal mol^{-1}) and C−H $\sigma \rightarrow$ Mo═S π^* (ΔE = 20.0 kcal mol^{-1}) back-donation are important in activating the substrate C−H bond for cleavage. Additional contributions to C−H activation derive from O_{eq} lp → C−H σ^* (lp = lone pair; ΔE = 8.2 kcal mol^{-1}) and S lp → C−H σ^* (ΔE = 13.2 kcal mol^{-1}) stabilizing interactions. The O_{eq}-donor ligand that derives from water is part of the Mo−O_{eq}−C fragment probed in the EPR spectra of inhibited XO, and the observation of O_{eq} lp → C−H σ^* back-donation indicates a key role for O_{eq} in activating the substrate C−H bond for cleavage. We also show that the O_{eq} donor plays an even more important role in TS stabilization. We find that O_{eq} → Mo + C charge transfer dominantly contributes to stabilization of the TS (ΔE = 89.5 kcal mol^{-1}) and the Mo−O_{eq}−C delocalization pathway reduces strong electronic repulsions that contribute to the classical TS energy barrier. The Mo−O_{eq}−C delocalization at the TS allows for the TS to be described in valence-bond terms as a resonance hybrid of the reactant (R) and product (P) valence-bond wave functions.

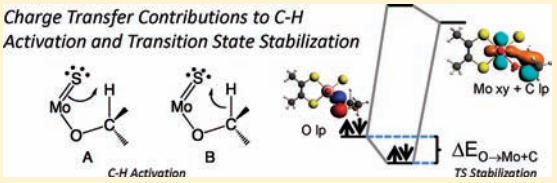

INTRODUCTION

Xanthine oxidoreductase (XO) is a molybdenum hydroxylase and the prototypical member of the XO pyranopterin molybdenum enzyme family.[1,2] XO catalyzes the oxidative hydroxylation of a wide variety of substrates, including purines and other aromatic heterocycles, aldehydes, and formamide by formal oxygen-atom insertion into the substrate C−H bond. A key difference between the molybdenum hydroxylases and monooxygenase enzymes is that the inserted oxygen atom derives from metal-activated water instead of dioxygen, and reducing equivalents are generated rather than consumed in the reductive half-reaction.[3] Both XO and the structurally related aldehyde oxidase (AO) have been implicated in prodrug activation and drug metabolism.[4−9] Although little is known regarding the pathophysiological relevance of AO,[10] the enzyme catalyzes the reduction of sulfa drugs, activates anticancer prodrugs,[11] and has recently been shown to metabolize famciclovir to the potent antiviral penciclovir,[12,13] which has been found to be effective against such viral infections as herpes simplex (types 1 and 2), Epstein−Barr, varicella zoster, and hepatitis B.[14] The structure of the oxidized XO active site (XO_{ox}) is five-coordinate square-pyramidal (Figure 1A) with an apical oxo ligand and equatorial sulfido, hydroxyl, and pyranopterin dithiolene sulfur ligands.[2,15−18] It is now generally believed that substrate hydroxylation is initiated by the nucleophilic attack of metal-activated water (i.e., hydroxide) on the substrate carbon atom that is to be hydroxylated, and this results in a tetrahedral intermediate (IM; Figure 1B) or transition state (TS; Figure 1C).[1,2,15,19,20] This mechanistic hypothesis is supported by spectroscopic and structural studies on enzyme−product complexes that confirm a Mo−O_{eq}−$C_{product}$ linkage.[15,21] A large kinetic isotope effect is observed upon deuteration of the C_8−H position of xanthine, and this is consistent with at least partial $C_{substrate}$−H bond breaking occurring at the TS.[22] This $C_{substrate}$−H bond-breaking step has been described as a transfer of hydride from the substrate to the sulfido (S^{2-}) ligand at the active site, resulting in a two-electron reduction of Mo^{VI} and protonation of the terminal sulfido (Figure 1D). The transfer of a hydride is of keen interest with respect to how large electronic repulsions and charge buildup associated with the sulfido−hydride interaction are compensated for along the reaction coordinate. Here we present a detailed electron paramagnetic resonance (EPR) and computational study of a key paramagnetic form of xanthine oxidase (XO) that serves as a basis for understanding important active site−substrate interactions along the reaction coordinate from the IM to the TS.

Received: July 12, 2011
Published: October 05, 2011

dx.doi.org/10.1021/ic201477n | Inorg. Chem. 2011, 50, 10919–10928

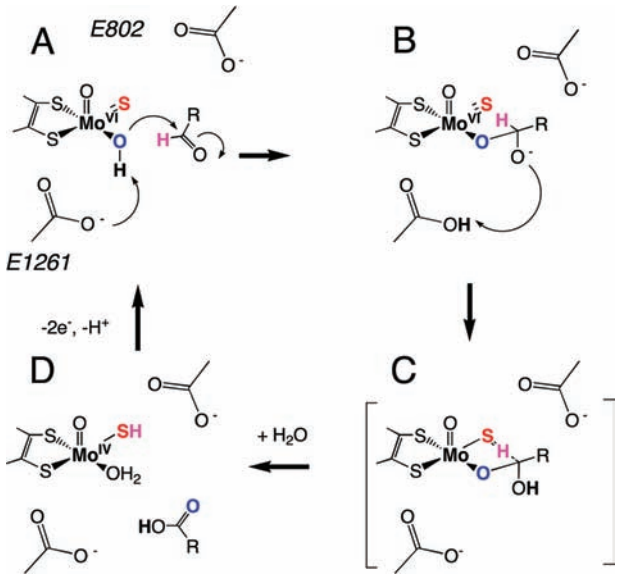

Figure 1. Proposed reaction mechanism for XO: (A) oxidized active site, (B) IM resulting from the nucleophilic attack of metal-activated water (i.e., HO^-) on the aldehyde carbonyl carbon and proton transfer to the general base E1261, (C) putative TS showing hydrogen migration between the substrate carbon and the terminal sulfido ligand, and (D) the reduced Mo^{IV} site following product release and binding of H_2O.

This paramagnetic Mo^V form of XO can be generated using aldehyde substrates to generate the aldehyde-inhibited enzyme form. Aldehyde-inhibited XO has been shown to exhibit ^{17}O, ^{33}S, ^{13}C, and $^{1,2}H$ hyperfine coupling with the Mo^V spin = $^1/_2$ center,[23−26] and Bray and co-workers suggested two structures for inhibited XO that possess tetrahedral carbon centers (Figure 2). Recent $^{1,2}H$ ENDOR studies on formaldehyde-inhibited XO have provided evidence for structure B in Figure 2.[27] Inhibited XO possesses structural features that are common to the putative IM and other nonplanar substrate carbon geometries along the reaction coordinate that we, and others,[19,20,28,29] have calculated for XO with aldehyde and heterocyclic aromatic organic (i.e., purine) substrates. These include the presence of Mo−S−R(H) ligation in place of a terminal sulfido (Mo═S), an Mo−O−R linkage, and a tetrahedral carbon center that derives from the aldehyde substrate. Thus, inhibited XO can be thought to represent a rudimentary *paramagnetic analogue* of enzyme structures found between the IM and the TS (Figure 1).

The relationship between the **g**, the $^{95,97}Mo$ hyperfine ($\mathbf{A}^{Mo}$), and the ^{13}C hyperfine ($\mathbf{A}^{C}$) tensors in aldehyde-inhibited XO has been used to understand the electronic origin of key delocalizations within the $Mo-O_{eq}-C$ fragment. These experimental data have been used to interpret the results of detailed bonding calculations for XO at geometries between the IM and the TS. Our combined spectroscopic and bonding study has provided new insight into the nature of the hydride-transfer process in XO family enzymes. We have used a natural bond orbital (NBO) formalism to show how specific donor−acceptor interactions contribute to C−H bond activation/cleavage and TS stabilization. The results highlight the importance of $Mo-O_{eq}-C$, C−H, and $Mo-S_{sulfido}$ bond covalency in mediating efficient electronic communication between the substrate and the molybdenum center and have allowed us to develop a valence-bond description of C−H activation and TS stabilization along the reaction coordinate with aldehyde substrates.

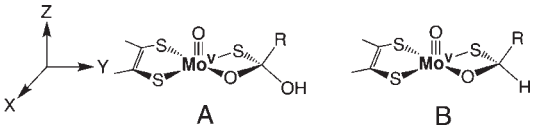

Figure 2. Structures originally proposed by Bray and co-workers for aldehyde-inhibited XO that possesses a tetrahedral carbon center. Recent ENDOR studies provide evidence for structure B.[27]

EXPERIMENTAL SECTION

Enzyme Preparation for Spectroscopic Studies. *Bos taurus* XO either was purchased from Sigma Aldrich or was isolated and purified from unpasteurized cow's milk according to the method of Massey and co-workers.[30,31] Both commercial and isolated XO samples had an A_{280}/A_{450} ratio of about 11.7 in a bicine/NaOH buffer, pH 8.2, and had an activity to flavin ratio (AFR) of 200 (a fully functional enzyme reported by Massey et al. had an AFR of 210 and an A_{280}/A_{450} ratio of about 5.3−5.8).[32] Enzyme concentrations were determined using the extinction coefficient at 450 nm (37 800 M^{-1} cm^{-1}). The inhibited enzyme form was generated using the reducing substrates formaldehyde, acetaldehyde, 2-pyridinecarboxaldehyde, and 3-pyridinecarboxaldehyde (Sigma Aldrich). XO was dialyzed against a 50 mM bicine/NaOH buffer at pH 8.2. XO samples (0.07−0.1 mM) were placed in quartz EPR tubes, and a large excess of the substrate (0.03−0.06 M) was then added. This mixture was then bubbled gently with oxygen with frequent shaking. These reaction mixtures were then incubated for times that ranged from minutes to hours depending on the nature of the substrate. Samples were then frozen in liquid N_2 for EPR measurements after appropriate incubation times.

EPR Spectroscopy. EPR spectra of XO were collected at X band (9.4 GHz) using a Bruker EMX spectrometer with associated Bruker magnet control electronics and microwave bridges. A microwave power of 20 dB was used for all experiments. Spectra were collected at 40 and 100 K using an Oxford Instruments liquid-helium-flow cryostat. Simulations of the EPR spectra were performed using the *MATLAB* toolbox *EasySpin*,[33] with further analyses performed using in-house written scripts for the program *Visual Molecular Dynamics*.[34]

Electronic Absorption Spectroscopy. Electronic absorption spectra were collected using a Hitachi U-3501 UV−vis−near-IR dual-beam spectrometer capable of scanning a wavelength region between 185 and 3200 nm. XO enzyme samples (∼5 μM) were incubated with aldehyde substrates (1 mM) in a 50 mM bicine/NaOH buffer solution at pH 8.2. The electronic absorption spectra were measured in a 1-cm-path-length, 100-μL, black-masked, quartz cuvette (Starna Cells, Inc.) equipped with a Teflon stopper. All electronic absorption spectra were collected at room temperature.

Computational Methods. Spin-unrestricted gas-phase geometry optimization calculations for two "inhibited" structures were performed at the density functional level of theory (DFT) using the *ORCA*,[35] *ADF*,[36] and *Gaussian 03W*[37] software packages. All *Gaussian 03W* calculations employed the B3LYP hybrid exchange-correlation functional.[38] A 6-31G(d,p) basis set, a split valence basis set with added polarization functions, was used for all atoms except molybdenum, where the LANL2DZ basis set, which includes an effective core potential, was used. The tetrahedral computational models for the aldehyde-inhibited structures were those originally proposed by Bray: for **1** [(dt)MoO(SC(R)(H)O)] and for **2** [(dt)MoO(SC(R)(OH)O)], where dt = 1,2-dimethyl-1,2-dithioethene and R = H, methyl, 2-pyridine, or 3-pyridine (Figure 2). Input files were prepared using GaussView or ADFInput, as appropriate. EPR parameters were calculated at

dx.doi.org/10.1021/ic201477n |*Inorg. Chem.* 2011, 50, 10919–10928

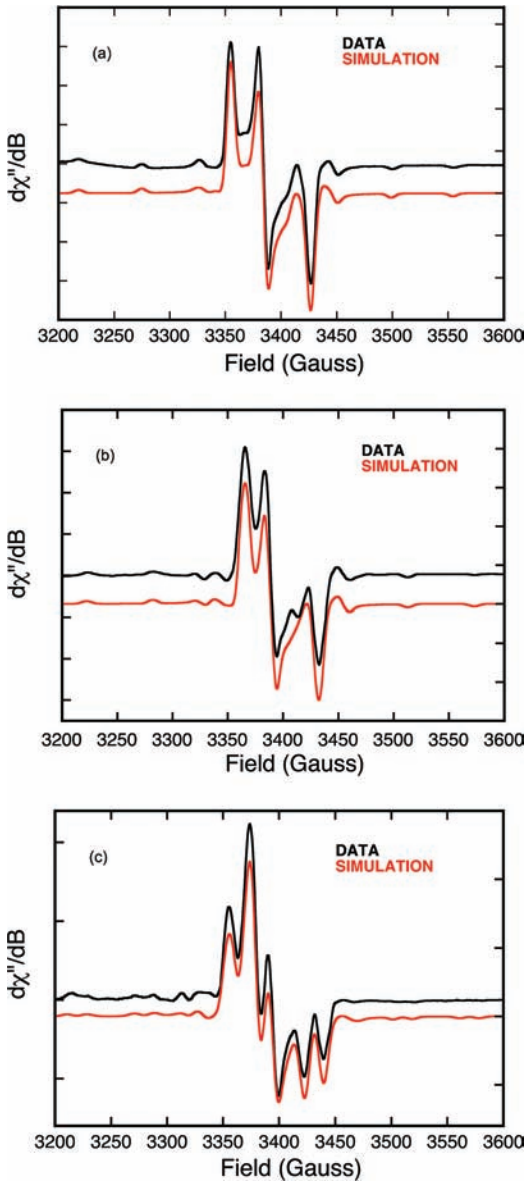

Figure 3. Aldehyde-inhibited X-band (9.41 GHz) EPR spectra for XO (0.07 mM) in a 50 mM bicine/NaOH buffer at pH 8.2. The aldehyde substrates are 3-pyridinecarboxaldehyde (a), HCOH (b), and $H^{13}COH$ (c). Experimental spectra are in black, and spectral simulations are in red. Spin-Hamiltonian parameters are given in Table 1.

the B3LYP/TZVP/ZORA[38−41] level using *ORCA 2.7.0*.[35,42,43] EPR calculations used a decontracted basis set and increased radial integration accuracy for molybdenum (specialgridintacc set to 7). *ADF* calculations used a triple-ζ basis set (TZP in the ADF basis set notation) and the Perdew−Burke−Ernzerhof[44] generalized gradient approximation density functional. Relativistic corrections were incorporated self-consistently in the *ADF* and *ORCA* calculations with the ZORA scalar relativistic Hamiltonian.[45,46] *ADF* geometry calculations (geometry optimizations, TS searches, and intrinsic reaction coordinates, IRCs) used frozen-core basis sets (C 1s, O 1s, S 1s2s2p, and Mo 1s2s2p3s4p) and default integration accuracies. Optimized geometries run as single-point calculations used no frozen cores and increased integration accuracy (integration key set to 6).

Reaction path geometries were located as follows (using *ADF2010*): first, a TS guess was located with a linear transit run and then converged with a TS search. The TS was verified by observation of a single large (-572 cm^{-1}) negative eigenvalue in the frequency calculation; this corresponded to the C−H stretching mode. The TS geometry and Hessian were then used as inputs for an IRC calculation. Selected IRC path points were then run as single-point jobs, and NBO analysis was performed using the *adfnbo* package.

RESULTS AND DISCUSSION

Nature of the Ground-State Wave Function for the Aldehyde-Inhibited Form of XO. Low-temperature (100 K) X-band (~9.4 GHz) EPR spectra for aldehyde-inhibited bovine XO using formaldehyde and 3-pyridinecarboxaldehyde are shown in Figure 3 (black). The data for 3-pyridinecarboxaldehyde-inhibited XO display well-resolved ^{95,97}Mo hyperfine splitting. The formaldehyde-inhibited EPR spectrum shows evidence for ^{1}H coupling, which results in increased spectral line broadening. Additionally, the formaldehyde-inhibited EPR spectrum displays ^{95,97}Mo ($I = {}^{5}/_{2}$) hyperfine splitting and well-resolved ^{13}C ($I = {}^{1}/_{2}$) hyperfine splitting when using $H^{13}COH$. The rhombic nature of the **g**-tensor anisotropy necessitates the use of an orthorhombic or lower-symmetry spin Hamiltonian in simulations of the EPR spectra (eq 1).

$$H = \mathbf{g}\beta B\cdot\hat{S} + \sum_{n=\mathrm{Mo,\,H,\,C}} \hat{I}\cdot\mathbf{A}^{n}\cdot\hat{S} \qquad (1)$$

Here, **g** is the **g** tensor, β is the Bohr magneton, B is the applied magnetic field, $\mathbf{A}^n$ are the nuclei-specific hyperfine coupling tensors (n = ^{95,97}Mo, ^{1}H, ^{13}C), $\hat{S}$ is the electron-spin operator, and $\hat{I}$ is the nuclear-spin operator. The ^{95,97}Mo and ^{13}C hyperfine tensors, $\mathbf{A}^{Mo}$ and $\mathbf{A}^{C}$, are comprised of an isotropic Fermi contact term, A^n_{iso}, a spin dipolar term, A^n_S, and an orbital dipolar term, A^n_L, the latter of which is typically small.[47] Although A^n_{iso} is proportional to the spin density at the nucleus of interest, the nature of the anisotropic A^n_S term results from the spatial distribution of the spin density around the nucleus. Therefore, the anisotropy in A^n_S contains important information regarding the delocalized nature of the singly occupied molecular orbital (SOMO) wave function and the electronic communication between the molybdenum center and a tetrahedral carbon center.[47]

Spectral simulations of the inhibited EPR spectra are presented in Figure 3 (red) and the relevant spin-Hamiltonian parameters given in Table 1. Formaldehyde-inhibited XO displays a strongly coupled proton[48,49] that is not evident in the 3-pyridinecarboxaldehyde spectra, and this indicates that the aldehydic R group is oriented in the "up" or M≡O direction (Figure 2). A previous inhibited EPR study utilized a ^{95,97}Mo isotope perturbation to obtain the hyperfine parameters A^{Mo}_{iso} = 42.72 × 10^{-4} cm^{-1} and A^{Mo}_S = [+9.83, −19.67, +9.83] × 10^{-4} cm^{-1}.[48] The anisotropy in the dipolar term A^{Mo}_S is unusual and indicative of a Mo(z^2) SOMO wave function.[50] In order to better understand the nature of the inhibited SOMO, we have determined the relative orientation of the **g** and $\mathbf{A}^{Mo}$ tensors. We note that the structure of the inhibited XO as presented in Figure 2 possesses a pseudo mirror plane ($y-z$) that bisects the dithiolene sulfur donors and contains the Mo≡O unit. Detailed EPR studies on Tp*$MoOX_2$ (X = F, Cl, Br) oxomolybdenum complexes that possess C_s (mirror) symmetry show that an increase in the molybdenum ligand covalency results in progressively larger rotations of the **g** tensor relative to $\mathbf{A}^{Mo}$ in the mirror plane.[51] Furthermore, C_s Tp*MoO(bdt) (bdt = benzene-2,3-dithiolate) also displays large rotations (~45°) of the **g** tensor

dx.doi.org/10.1021/ic201477n |*Inorg. Chem.* 2011, 50, 10919–10928

Table 1. EPR Parameters for Inhibited XO (Bovine)[a]

parameters	axis			average	Euler angles (*zyz*)		
	z	*y*	*x*	⟨*A*⟩	*α*	*β*	*γ*
			Formaldehyde				
g	2.0002 (1.9972)	1.9856 (1.9802)	1.9610 (1.9525)	1.9823 (1.9766)			
$A(^{95,97}\text{Mo};\ \times 10^{-4}\ \text{cm}^{-1})$	59.50 (54.14)	23.00 (18.45)	22.50 (17.97)	35.00 (30.19)	86.75°	138.59°	8.28°
$A(^{13}\text{C};\ \times 10^{-4}\ \text{cm}^{-1})$	12.33 (11.34)	16.67 (11.69)	16.00 (14.72)	15.00 (12.58)	90.00°	69.15°	56.58°
$A(^{1}\text{H};\ \times 10^{-4}\ \text{cm}^{-1})$	3.33 (3.65)	3.33 (3.97)	5.00 (5.84)	3.89 (4.49)	9.51°	102.89°	−81.87°
			2-Pyridinecarboxaldehyde				
g	2.0025 (1.9997)	1.9878 (1.9812)	1.9614 (1.9559)	1.9839 (1.9789)			
$A(^{95,97}\text{Mo};\ \times 10^{-4}\ \text{cm}^{-1})$	57.00 (53.99)	22.33 (18.52)	21.67 (17.80)	33.67 (29.65)	69.00°	137.00°	17.62°
			3-Pyridinecarboxaldehyde				
g	1.9995 (2.0001)	1.9824 (1.9815)	1.9578 (1.9570)	1.9799 (1.9795)			
$A(^{95,97}\text{Mo};\ \times 10^{-4}\ \text{cm}^{-1})$	56.33 (53.59)	20.67 (18.10)	20.67 (17.26)	32.33 (29.65)	72.00°	140.00°	12.00°

[a] Parameters in parentheses are the calculated spin-Hamiltonian parameters. Euler rotations are defined as a rotation of the g_i axes relative to the *A*-axis frame. Using a right-hand coordinate frame, the rotation α is about the A_z axis, the rotation β is about the new *y* axis, and the rotation γ is about the new *z* axis. A counterclockwise rotation is positive. EPR parameters were calculated at the B3LYP/TZVP/ZORA[40] level using *ORCA 2.7.0*.[35,42,43]

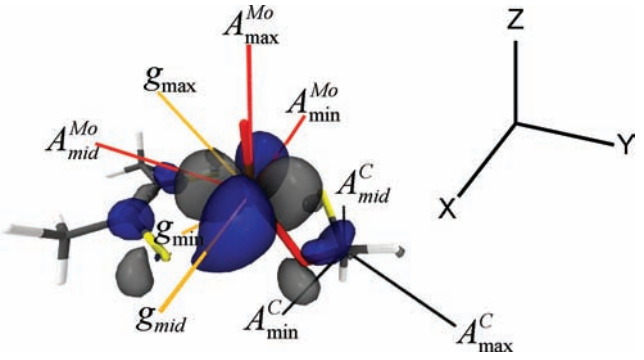

Figure 4. Calculated principal-component orientations of the **g**, $\mathbf{A}^{Mo}$, and $\mathbf{A}^{C}$ tensors for inhibited XO superimposed on the DFT-calculated β lowest unoccupied molecular orbital (β-LUMO) wave function. The largest component of $\mathbf{A}^{Mo}$ (A^{Mo}_{max}) is oriented 4.75° off of the Mo≡O bond. The largest component of $\mathbf{A}^{C}$ (A^{C}_{max}) forms a 160° angle with A^{Mo}_{mid} (see the text).

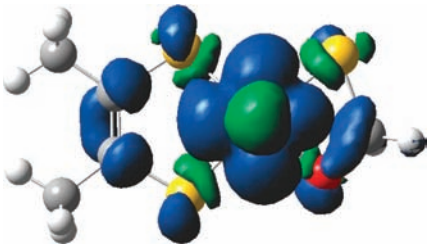

Figure 5. Calculated spin-density distribution for **1**. The orientation is down the *z* axis of Figure 4. Positive spin density (blue) is delocalized from the molybdenum center onto O_{eq} and the tetrahedral carbon. Negative spin density (green) is found on S_{eq}. Calculated atomic spin populations: Mo = +99.5%; S_{eq} = −0.57%; C = +2.03%; O_{eq} = +1.91%.

relative to $\mathbf{A}^{Mo}$ in the mirror plane of this molecule.[52,53] We note that, in C_s symmetry, one component of the **g** and $\mathbf{A}^{Mo}$ tensors is collinear (*x* direction).[50] All of our EPR simulations for inhibited XO were obtained with Euler rotations (i.e., β) that primarily rotate the **g** tensor in the molecular *y*−*z* plane relative to $\mathbf{A}^{Mo}$. This results in principle components of A^{Mo}_{S} that indicate a normal Mo(x^2-y^2) ground state for inhibited XO, with the Mo(x^2-y^2) redox orbital oriented orthogonal to the Mo≡O bond. The nature of the $\mathbf{A}^{C}$ tensor is consistent with spin being delocalized from the molybdenum center to the C(sp_y) hybrid atomic orbital that derives from the carbonyl carbon of the aldehyde substrate. The orientation of A^{Mo}_{mid} relative to the molecular frame places A^{Mo}_{mid} along the lobes of the Mo(x^2-y^2) orbital that bisect the dithiolene S_{dt} donors and point in the general direction of the tetrahedral carbon center (Figure 4). The calculated angle between A^{Mo}_{mid} and A^{C}_{max}, the largest component of A^{C}_{S}, is 160°, and this defines the relative orientation of the Mo(x^2-y^2) and C(sp_y) orbitals with respect to each other. The deviation from 180° is indicative of asymmetry within the Mo(−O−C−S−) four-membered chelate ring. Calculations reveal nonzero Mo−C, Mo−O_{eq}, and O_{eq}−C overlaps in the singly occupied Mo(x^2-y^2) wave function. These nonzero overlaps provide a potentially direct pathway for Mo → C spin delocalization[27] as well as a covalent delocalization pathway mediated by the Mo−O_{eq}−C linkage. However, despite the fact that the Mo(x^2-y^2) and C(sp_y) orbitals are aligned for a potential net pseudo-σ-bonding interaction, the calculated Mo−C Mayer bond order[54] in inhibited XO is zero.

Spin-Population Analysis and Metal−Ligand Covalency. The good agreement between the calculated and experimental ^{95,97}Mo hyperfine, ^{13}C hyperfine, and **g** tensors, as well as the relationship between their experimentally determined Euler rotational matrices (Table 1 and Figure 4), allows us to explore the electronic origin of these parameters in inhibited XO in terms of the calculated spin densities and atomic spin populations. We recently used this procedure to calibrate the experimentally determined nitrogen hyperfine interaction (hfi) with calculated nitrogen atomic spin populations on the acceptor fragment in a series of donor−acceptor biradical systems.[55] An excellent correlation was obtained between the calculated nitrogen spin populations and the experimentally determined hfi's, and this was evaluated in the context of detailed bonding calculations, which provided insight into the electronic origins of covalent spin

dx.doi.org/10.1021/ic201477n |*Inorg. Chem.* 2011, 50, 10919–10928

delocalization and spin polarization contributions to the observed nitrogen hfi's. Specifically, this work showed that the nature of the spin-density distribution can serve as a probe of donor → acceptor and, by inference, ligand-to-metal charge transfer (LMCT).

Inspection of the calculated spin densities (Figure 5) and atomic spin populations in inhibited XO shows covalent delocalization of positive spin from the Mo^{V} d^1 center onto the O_{eq} and carbon centers of the four-membered chelate ring. The observation of net positive spin populations on oxygen and carbon contrasts with the *negative* net spin population on the equatorial chelate ring sulfur donor (S_{eq}). The observation of a net negative spin population on S_{eq} is unusual and derives from a spin-polarization mechanism, which results from the configurational mixing of S_{eq} → Mo LMCT states that are formed from promotion of an α (spin-up) electron localized in a doubly occupied molecular orbital to an unoccupied virtual orbital localized on molybdenum. S_{eq} → Mo LMCT transitions will only contribute to positive spin populations on S_{eq} if the acceptor orbital in these S_{eq} → Mo LMCT transitions is the half-occupied $Mo(x^2-y^2)$ acceptor orbital. This idea is supported by our calculated LMCT oscillator strengths for inhibited XO, which indicate the absence of intense (i.e., $\varepsilon > 400\ M^{-1}\ cm^{-1}$), low-energy ($E < 22\,000\ cm^{-1}$) $S_{eq} \rightarrow Mo(x^2-y^2)$ LMCT transitions. The observation of a negative spin population on S_{eq} is also consistent with the small degree of $Mo(x^2-y^2)-S_{eq}$ covalency calculated for inhibited XO, where the spin-bearing α-HOMO (HOMO = highest occupied molecular orbital) possesses <2% $S_{eq}(p)$ character. The $O_{oxo}-Mo-S_{eq}-C$ dihedral angle in inhibited XO is calculated to be ~107.0°, and this geometry precludes dominant $Mo(x^2-y^2)-S_{eq}(p)$ π-type orbital interactions because the in-plane ($x-y$ plane) $S_{eq}(p)$ orbital capable of forming a π bond with molybdenum is involved in strong σ bonding with the chelate ring carbon.[56,57] Such low $Mo-(x^2-y^2)-S_{thiolate}$ covalency in oxomolybdenum thiolate is rare but has recently been realized in Tp*MoO(mba) (mba = mercaptobenzyl alcohol), which possesses a 95.5° $O_{oxo}-Mo-S_{thiolate}-C$ dihedral angle.[58] Detailed S K-edge X-ray absorption spectroscopy (XAS) studies have provided an experimental estimate of ~0% sulfur thiolate character admixed into the molybdenum redox orbital of Tp*MoO(mba).[58] Thus, the low $Mo(x^2-y^2)-S_{eq}$ covalency found in inhibited XO is a direct consequence of the $O_{oxo}-Mo-S_{eq}-C$ dihedral angle, which precludes any appreciable $Mo(x^2-y^2)-S_{eq}(p)$ π-type covalency. In marked contrast to the <2% $S_{eq}(p)$ character admixed into the inhibited spin-bearing α-HOMO, the O_{eq} donor contributes ~10% character to this orbital. Therefore, the $Mo(x^2-y^2)-O_{eq}$ bond covalency in inhibited XO, coupled with the structural similarities between inhibited XO and XO along the IM → TS reaction coordinate, points to a potentially important role for O_{eq} in (1) C−H bond activation and (2) electronic communication between the molybdenum and carbon centers along the reaction coordinate via a direct $Mo(x^2-y^2)-O_{eq}-C$ pathway.

Role of Mo−S, Mo−O_{eq}−C, and C−H Donor−Acceptor Interactions in C−H Bond Activation and TS Stabilization. The calculated spin densities and atomic spin populations for inhibited XO reveal a covalent spin-delocalization pathway that involves the molybdenum ion, O_{eq}, and the tetrahedral carbon center. The observation of this delocalization, coupled with the structural similarity between inhibited XO and active-site structures that evolve along the IM → TS reaction coordinate, has spurred our interest in electronic structure contributions to the XO reaction coordinate with aldehyde substrates. The IM → TS activation energy, ΔE^{+}, calculated with acetaldehyde as the substrate is found to be 12.6 kcal mol^{-1}, and the IM → TS reaction profile as a function of the acetaldehyde C−H distance is presented in Figure 6. The results for the IM → TS reaction profile are in general agreement with those obtained using detailed quantum mechanical/molecular mechanics approaches.[19] A key question that has remained unanswered regarding electronic structure contributions to the reactivity in XO relates to how the enzyme facilitates activation and scission of the substrate C−H bond along the reaction coordinate. In order to address this issue, we have employed an NBO analysis, which provides insight into electronic structure contributions to C−H activation and key charge-transfer stabilizations that lead to a reduction in the repulsive interactions along the reaction coordinate and, ultimately, to a lowering of the activation energy for enzymatic aldehyde oxidation.

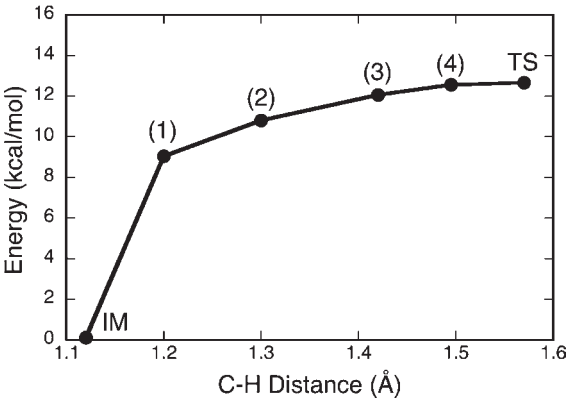

Figure 6. Calculated energy profile along the reaction coordinate from IM to TS as a function of the substrate (acetaldehyde) C−H distance. Note that the charge of the transferred hydrogen is positive and does not change along this coordinate, in agreement with prior work.[19]

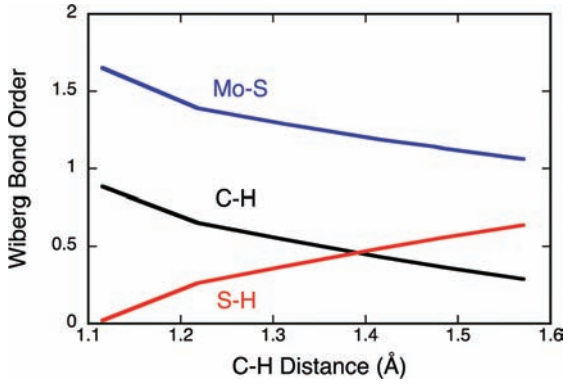

Figure 7. Wiberg bond orders[60] calculated along the reaction coordinate of Figure 6: blue, Mo═S; black, C−H; red, S−H.

NBOs conveniently represent localized lone-pair and bonding regions[59] and provide a convenient way to develop a valence-bond, or Lewis structure, description of important bonding interactions along the IM → TS reaction coordinate in XO-catalyzed oxidations. In order to reach the TS and ultimately form product (P), the C−H σ and Mo═S π bonds must be broken concomitantly with formation of an S−H σ bond and

dx.doi.org/10.1021/ic201477n |*Inorg. Chem.* 2011, 50, 10919–10928

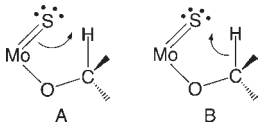

Figure 8. Lewis structures that describe Mo=S $\pi \rightarrow$ C−H σ^* charge transfer resulting in S−H bond formation (A) and C−H $\sigma \rightarrow$ Mo=S π^* charge transfer resulting in S−H bond formation (B).

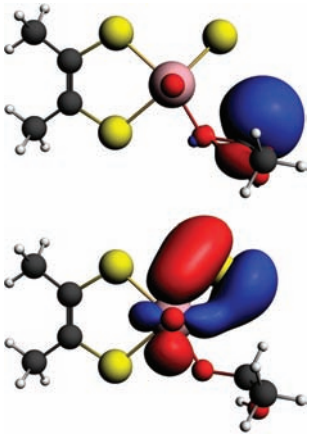

Figure 9. NBOs for the C−H σ bond (top) and the Mo=S π bond (bottom) at the IM geometry.

reduction of the Mo^{VI} state to Mo^{IV}. The calculated Wiberg bond order[60] changes for the Mo=S, C−H, and S−H bonds along the IM → TS reaction coordinate are presented in Figure 7 and clearly reflect these key bond-making and bond-breaking steps. Reducing the aldehyde C−H bond order and activating this bond for cleavage can involve electron occupation of the C−H σ^*-antibonding orbital (Figure 8A) or a reduction of the electron density in the C−H σ-bonding orbital (Figure 8B). Therefore, it is of interest to evaluate the relative contributions of the complementary charge-transfer interactions in Figure 8 to C−H activation and eventual TS stabilization. The calculated C−H σ-bonding and Mo=S π-bonding NBOs for XO at the IM geometry are presented in Figure 9, and occupation numbers are given in Table 2. The C−H bonding interaction is formed from C(2p)−H(1s) orbital overlap. Because the H(1s) orbital possesses no radial nodes, the resulting heteronuclear diatomic-type NBO takes on the appearance of an atomic s−p hybrid orbital. Both the C−H σ-bonding and C−H σ-antibonding NBOs possess large amplitudes on the C−H hydrogen atom with a larger radial extension observed for the C−H σ-antibonding orbital. The Mo=S π-bonding NBO is very covalent, with approximately 60% sulfur and 40% molybdenum character, while the corresponding Mo=S π^*-antibonding NBO possesses 40% sulfur and 60% molybdenum character. The nature of the Mo=S π^*-antibonding NBO is in excellent agreement with the results of S K-edge XAS studies on the molybdenum(VI) model compound $Tp^{i\text{-}Pr}MoOS(OPh)$, which showed 30−41% sulfido character in the oxidized LUMO (Mo=S π^*) wave function.[61] The Mo(4d)−S(3p) interaction that comprises the Mo=S bonding scheme results in a high degree of covalency due to the large radial expansion of the Mo(4d) and S(3p) atomic orbitals and the small energy difference between these orbitals. This results in a calculated Mo=S π−Mo=S π^* energy gap at the IM geometry

Table 2. NBO Occupation Numbers for Points IM to 3

point	C−H σ	C−H σ^*	Mo−S π	Mo−S π^*	O_{eq} lp	S lp
IM	1.97e	0.06e	1.92e	0.23e	1.66e	1.99e
1	1.80e	0.18e	1.89e	0.42e	1.67e	1.97e
2	1.73e	0.24e	1.87e	0.51e	1.67e	1.97e
3	1.63e	0.32e	1.84e	0.60e	1.65e	1.96e

of only 21 350 cm^{-1} (2.7 eV). Thus, the Mo=S bonding scheme represents a unique electronic structure poised to activate substrate C−H bonds through C−H $\sigma \rightarrow$ Mo=S π^* and Mo=S $\pi \rightarrow$ C−H σ^* donations, with both reducing the C−H bond order and activating this bond for cleavage.

Figure 10 displays key bonding (b) and lone-pair (lp) donor NBOs (left on each donor−acceptor orbital diagram) and antibonding (ab*) acceptor NBOs (right on each donor−acceptor orbital diagram) for point 2 along the reaction coordinate of Figure 6. Here, the substrate hydrogen being transferred to the terminal sulfido ligand is approximately midway between the C−H distance of the IM and the C−H distance in the TS. The stabilization energy (ΔE) resulting from these bonding interactions can be approximated using second-order perturbation theory via[59]

$$\Delta E^{(2)} = -2\frac{\langle \mathrm{b(lp)}|\hat{F}|\mathrm{ab}^*\rangle^2}{E_{\mathrm{ab}^*} - E_{\mathrm{b(lp)}}} \quad (2)$$

where $\langle \mathrm{b(lp)}|\hat{F}|\mathrm{ab}^*\rangle$ is the Fock matrix element between the donor (b or lp) and acceptor (ab*) NBOs and $E_{\mathrm{ab}^*} - E_{\mathrm{b(lp)}}$ is the energy difference between a corresponding pair of donor and acceptor NBOs. The charge transferred, $Q_{\mathrm{b(lp)}\rightarrow\mathrm{ab}^*}$, between the donor and acceptor NBOs is defined as[59]

$$Q_{\mathrm{b(lp)}\rightarrow\mathrm{ab}^*} = \frac{\Delta E}{E_{\mathrm{ab}^*} - E_{\mathrm{(lp)}}} \quad (3)$$

The dominant donor → acceptor interactions that contribute to C−H bond activation derive from the Mo=S $\pi \rightarrow$ C−H σ^* (ΔE = 24.3 kcal mol^{-1}) and C−H $\sigma \rightarrow$ Mo=S π^* (ΔE = 20.0 kcal mol^{-1} interactions). Additional appreciable contributions originate from O_{eq} lp → C−H σ^* (ΔE = 8.2 kcal mol^{-1}) and S lp → C−H σ^* (ΔE = 13.2 kcal mol^{-1}) stabilizing interactions. Furthermore, the charge transfers derived from eq 2 show that, at position 2 along the reaction coordinate, 0.11e has been back-donated into the Mo=S π^* antibond from the C−H σ bond. A markedly larger 0.19e has been transferred into the C−H σ^* antibond from the Mo−S π bond and the S and O_{eq} lp orbitals because of a combination of Mo=S $\pi \rightarrow$ C−H σ^*, O_{eq} lp → C−H σ^*, and S lp → C−H σ^* charge-transfer interactions. Values for the calculated NBO occupation numbers, energy stabilizations, and Fock matrix elements at points IM and 1−3 are provided in Tables 2−4.

A covalency-induced "electronic buffer effect" has been observed in oxomolybdenum dithiolene model compounds.[62,63] This has been postulated to take advantage of the redox-noninnocent behavior of the coordinated dithiolene to modulate[64] the reduction potential of the molybdenum site during the course of catalysis via molybdenum dithiolene forward donation and back-donation. In the molybdenum hydroxylases, we find that similar charge-transfer stabilizations occur along the reaction coordinate that effectively buffer the active site against the large formal charge changes that accompany C−H bond cleavage.

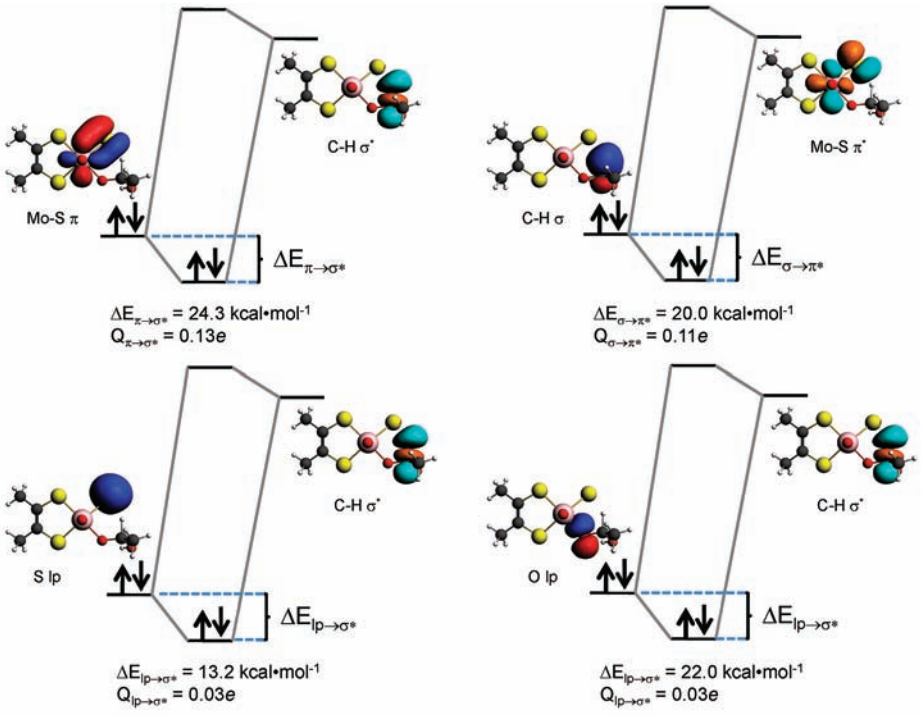

Figure 10. NBOs for point 2 showing charge-transfer energy stabilizations and charge transferred (Q) between the donor and acceptor NBOs.

Table 3. Donor → Acceptor Energy Stabilizations for Points IM to 3 (Energies in kcal mol^{-1})

point	C−H σ → Mo−S π^*	Mo−S π → C−H σ^*	O_{eq} lp → C−H σ^*	S lp → C−H σ^*
IM	0.08	0.73	4.6	<0.05
1	11.2	17.0	5.1	9.9
2	20.0	24.3	8.2	13.2
3	36.2	33.4	12.6	16.5

Table 4. Fock Matrix Elements (F_{ij}) and Energy Gaps (ΔE) for Points IM to 3

	C−H σ → Mo−S π^*		Mo−S π → C−H σ^*		O_{eq} lp → C−H σ^*		S lp → C−H σ^*	
point	F_{ij} (eV)	ΔE (eV)	F_{ij} (eV)	ΔE (eV)	F_{ij} (eV)	ΔE (eV)	F_{ij} (eV)	ΔE (eV)
IM	0.14	10.07	0.49	15.78	1.31	15.51		
1	1.50	8.16	2.12	11.97	1.36	15.51	2.37	24.22
2	1.91	7.35	2.37	10.07	1.55	12.79	2.67	22.04
3	2.40	6.53	2.56	8.44	1.71	10.61	2.88	19.86

Here, the key processes are the complementary forward donation from the C−H σ bond to Mo═S π^* and back-donation into C−H σ^* from the Mo═S π bond. This directly results from the highly covalent Mo═S bonding interaction[61] (Figure 9), which markedly reduces charge buildup on the transferred hydrogen and minimizes repulsive interactions along the C---H---S reaction coordinate.

With respect to the S−H bond-forming and C−H bond-breaking steps that were anticipated from Figure 8, the calculated C−H σ bond order is reduced to 0.29 at the TS, while the corresponding S−H σ bond order has increased to 0.64 (Figure 7). Additionally, the Mo═S bond order has been reduced from 1.65 at the IM to 1.06 at the TS because of a weakening of the Mo═S π bond. A weak Mo═S π-bonding interaction is still present at the TS, and this results from Mo − C → S−H σ^* back-donation, as depicted in Figure 11. Following these large changes in the bond order, the key question now shifts from how the C−H bond is activated to describing the nature of TS stabilization in XO. We note that the use of these interaction energies may not be quantitatively accurate for the description of TSs that are highly delocalized[65] because these NBO stabilization energies derive from a perturbative treatment. However, these energies can be used in a qualitative way to provide an intuitive description of the key donor−acceptor contributions to TS stabilization.

In contrast to earlier points (see 1−3 in Figure 6) along the reaction coordinate, the donor−acceptor interactions that dominantly contribute to the stabilization of point 4 and the TS are different. Important donor and acceptor NBOs and their respective donor−acceptor interactions at the TS are presented in Figure 11. The donor (Mo − C; 70% Mo/30% C) and acceptor (Mo + C; 30% Mo/70% C) NBOs are best described as linear combinations of the product (molybdenum lone-pair) and reactant (carbon lone-pair) orbitals. Here it is observed that the dominant donor → acceptor interaction that contributes to TS stabilization derives from the O_{eq} → Mo + C charge transfer (ΔE = 89.5 kcal mol^{-1}). The nature of the O_{eq}→ Mo + C charge-transfer interaction is important because it results in a nascent product C═O π-bonding interaction and it contributes to molybdenum reduction. The effects of this delocalization are clearly observed in the doubly occupied natural localized

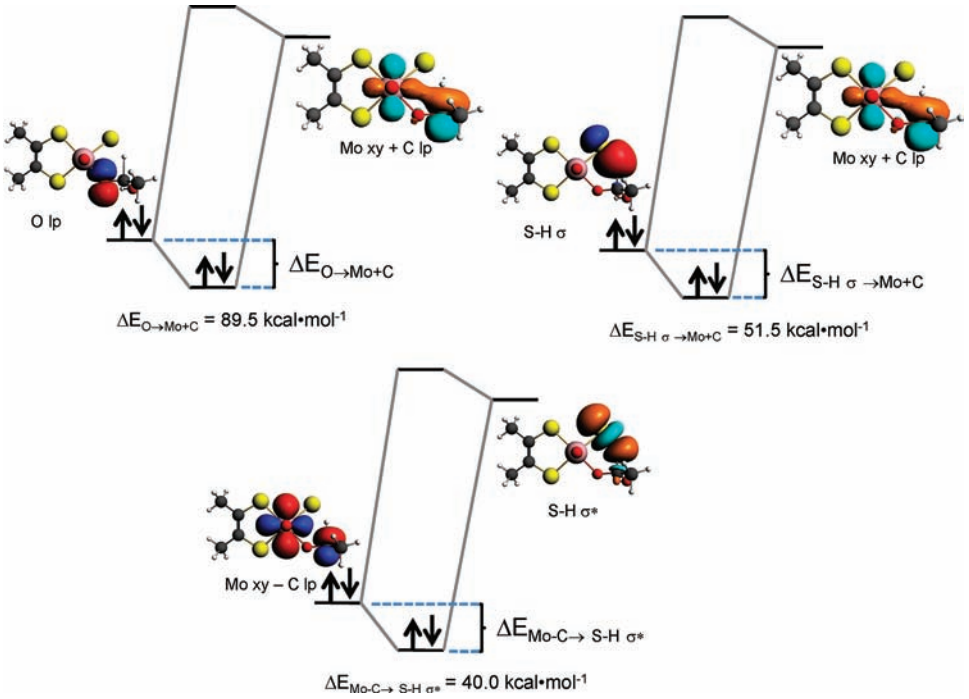

Figure 11. Charge-transfer energy stabilizations between donor and acceptor NBOs at the XO/XDH TS.

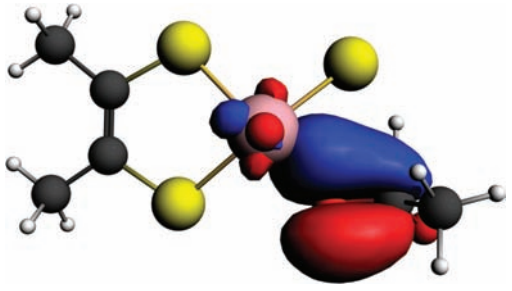

Figure 12. NLMO that derives from dominant $O_{eq} \rightarrow$ Mo + C charge transfer showing nacent C═O π bonding, leading to product formation.

molecular obital (NLMO) of Figure 12. We note that 95% of this NLMO derives from the $O_{eq} \rightarrow$ Mo + C charge-transfer interaction observed in Figure 11. Other stabilizing donor−acceptor interactions include S−H $\sigma \rightarrow$ Mo + C (ΔE = 51.5 kcal mol^{-1}) and the aforementioned Mo − C → S−H σ^* (ΔE = 40.2 kcal mol^{-1}) charge transfer that contributes to Mo═S π bonding.

Remarkably, the $O_{eq} \rightarrow$ Mo + C charge transfer results in the same type of Mo−O_{eq}−C delocalization that was described earlier in our analysis of the EPR-derived hfi's and the calculated positive spin-density delocalization in aldehyde-inhibited XO. That such similar Mo−O_{eq}−C delocalizations could be so important in stabilizing the TS in XO and promoting a positive spin population on the tetrahedral carbon center in inhibited XO supports our earlier statement that inhibited XO may be thought of as a rudimentary paramagnetic analogue of the TS. In addition to contributing to molybdenum reduction and product C═O π-bond formation, the $O_{eq} \rightarrow$ Mo + C charge transfer strongly contributes to a lowering of the energy of the TS. This results from the fact that this charge-transfer interaction effectively reduces the strong electronic repulsions present at the TS that contribute to the classical energy barrier, a concept that is central to TS theory.[59,66]

CONCLUSION

The $C_{substrate}$−H bond-breaking step in XO has been previously described as a transfer of hydride from the substrate to the sulfido (S^{2-}) ligand at the active site, resulting in a two-electron reduction of molybdenum(VI) and protonation of the terminal sulfido. Our interest in XO-mediated hydride transfer has been focused on how the enzyme reduces the large electronic repulsions and charge buildup associated with C−H bond scission along the reaction coordinate. We have used EPR spectroscopy to study an XO-inhibited enzyme form, and the results have been used to support detailed bonding calculations along the XO reaction coordinate. Our analysis of aldehyde-inhibited EPR spectra has yielded the relative orientations of the **g** and ^{95,97}Mo and ^{13}C hyperfine tensors. The anisotropy in the ^{95,97}Mo hyperfine tensor is now interpreted in terms of proper Euler rotations that support a Mo(x^2-y^2) ground state for this species. The calculated spin densities and atomic spin populations for inhibited XO have been used to highlight a key Mo−O_{eq}−C delocalization pathway that contributes to appreciable spin delocalization onto the tetrahedral carbon center that derives from the aldehyde substrate. NBO analysis of the XO reaction coordinate with acetaldehyde as the reducing substrate shows that the dominant donor → acceptor interactions that facilitate weakening and concomitant activation of the substrate C−H bond derive from Mo═S $\pi \rightarrow$ C−H σ^* and C−H $\sigma \rightarrow$ Mo═S π^* back-donations. These competing donor−acceptor interactions allow the substrate C−H hydrogen to be transferred to the terminal sulfido with only a slight positive charge, and this charge does not change along the reaction coordinate. An additional contribution originating from O_{eq} lp → C−H σ^*

dx.doi.org/10.1021/ic201477n |*Inorg. Chem.* 2011, 50, 10919–10928

charge transfer is also present. The O_{eq} donor plays an even more important role in TS stabilization. We find that the $O_{eq} \rightarrow Mo + C$ charge-transfer process dominantly contributes to TS stabilization. Thus, the $Mo-O_{eq}-C$ delocalization pathway observed in aldehyde-inhibited XO reduces strong electronic repulsions that contribute to the classical TS energy barrier in the enzyme. In summary, this work has increased our understanding of substrate C−H bond activation and the nature of through-bond donor−acceptor electronic couplings, which allows for efficient electronic communication between the substrate and molybdenum center along the XO reaction coordinate.

AUTHOR INFORMATION

Corresponding Author
*E-mail: mkirk@unm.edu.

ACKNOWLEDGMENT

M.L.K. acknowledges National Institutes of Health Grant GM 057378 for financial assistance.

REFERENCES

(1) Hille, R. *Arch. Biochem. Biophys.* **2005**, *433*, 107.
(2) Kirk, M. L.; Knottenbelt, S.; Habtegabre, A. In *Computational Inorganic and Bioinorganic Chemistry*; Solomon, E. I., Scott, R. A., King, B. R., Eds.; Wiley: New York, 2009; p 614.
(3) Hille, R. *Chem. Rev.* **1996**, *96*, 2757.
(4) Purifoy, D.; Beauchamp, L.; Demiranda, P.; Ertl, P.; Lacey, S.; Roberts, G.; Rahim, S.; Darby, G.; Kretinsky, T.; Powell, K. *J. Med. Virol.* **1993**, *S1*, 139.
(5) Demiranda, P.; Burnette, T. *Drug Metab. Dispos.* **1994**, *22*, 55.
(6) Fowles, S.; Pratt, S.; LaRoche, J.; Prince, W. *Eur. J. Clin. Pharmacol.* **1994**, *46*, 355.
(7) Krasny, H.; Beauchamp, L.; Krenitsky, T.; Demiranda, P. *Drug Metab. Dispos.* **1995**, *23*, 1242.
(8) Obach, R. S. *Drug Metab. Dispos.* **2004**, *32*, 89.
(9) Smith, M. A.; Marinaki, A. M.; Arenas, M.; Shobowale-Bakre, M.; Lewis, C. M.; Ansari, A.; Duley, J.; Sanderson, J. D. *Aliment. Pharmacol. Ther.* **2009**, *30*, 375.
(10) Garattini, E.; Mendel, R.; Romao, M. J.; Wright, R.; Terao, M. *Biochem. J.* **2003**, *372*, 15.
(11) Rooseboom, M.; Commandeur, J. N. M.; Vermeulen, N. P. E. *Pharm. Rev.* **2004**, *56*, 53.
(12) Hodge, R. *Antiviral Chem. Chemother.* **1993**, *4*, 67.
(13) Rashidi, M.; Smith, J.; Clarke, S.; Beedham, C. *Drug Metab. Dispos.* **1997**, *25*, 805.
(14) Hille, R. *J. Biol. Inorg. Chem.* **1996**, *1*, 397.
(15) Pauff, J. M.; Cao, H.; Hille, R. *J. Biol. Chem.* **2009**, *284*, 8751.
(16) Pauff, J. M.; Zhang, J. J.; Bell, C. E.; Hille, R. *J. Biol. Chem.* **2008**, *283*, 4818.
(17) Asai, R.; Nishino, T.; Matsumura, T.; Okamoto, K.; Igarashi, K.; Pai, E. F. *J. Biochem.* **2007**, *141*, 525.
(18) Enroth, C.; Eger, B.; Okamoto, K.; Nishino, T.; Nishino, T.; Pai, E. *Proc. Natl. Acad. Sci. U.S.A.* **2000**, *97*, 10723.
(19) Metz, S.; Thiel, W. *J. Am. Chem. Soc.* **2009**, *131*, 14885.
(20) Zhang, X. H.; Wu, Y. D. *Inorg. Chem.* **2005**, *44*, 1466.
(21) Hemann, C.; Ilich, P.; Stockert, A. L.; Choi, E. Y.; Hille, R. *J. Phys. Chem. B* **2005**, *109*, 3023.
(22) D'Ardenne, S.; Edmondson, D. *Biochemistry* **1990**, *29*, 9046.
(23) Howes, B.; Bennett, B.; Bray, R.; Richards, R.; Lowe, D. *J. Am. Chem. Soc.* **1994**, *116*, 11624.
(24) Howes, B.; Pinhal, N.; Turner, N.; Bray, R.; Anger, G.; Ehrenberg, A.; Raynor, J.; Lowe, D. *Biochemistry* **1990**, *29*, 6120.
(25) Morpeth, F.; George, G.; Bray, R. *Biochem. J.* **1984**, *220*, 235.
(26) Malthouse, J.; George, G.; Lowe, D.; Bray, R. *Biochem. J.* **1981**, *199*, 629.
(27) Shanmugam, M.; Zhang, B.; McNaughton, R. L.; Kinney, R. A.; Hille, R.; Hoffman, B. M. *J. Am. Chem. Soc.* **2010**, *132*, 14015.
(28) Alfaro, J. F.; Joswig-Jones, C. A.; Ouyang, W.; Nichols, J.; Crouch, G. J.; Jones, J. P. *Drug Metab. Dispos.* **2009**, *37*, 2393.
(29) Bayse, C. A. *Dalton Trans.* **2009**, 2306.
(30) Komai, H.; Massey, V.; Palmer, G. *J. Biol. Chem.* **1969**, *244*, 1692.
(31) Hille, R.; Kim, J. H.; Hemann, C. *Biochemistry* **1993**, *32*, 3973.
(32) Massey, V.; Komai, H.; Palmer, G.; Elion, G. B. *J. Biol. Chem.* **1970**, *245*, 2837.
(33) Stoll, S.; Schweiger, A. *J. Magn. Reson.* **2006**, *178*, 42.
(34) Humphrey, W.; Dalke, A.; Schulten, K. *J. Mol. Graph.* **1996**, *14*, 33.
(35) Neese, F. *ORCA, an ab initio, density functional, and semi-empirical program package*; University of Bonn: Bonn, Germany, **2009**.
(36) ADF2009.01 SCM, Theoretical Chemistry, Vrije Universiteit, Amsterdam, The Netherlands, http://www.scm.com.
(37) *Gaussian 03*; RCG, Inc.: Pittsburgh, PA, 2003.
(38) Becke, A. *J. Chem. Phys.* **1993**, *98*, 5648.
(39) van Lenthe, E.; Baerends, E. J.; Snijders, J. G. *J. Chem. Phys.* **1994**, *101*, 9783.
(40) Weigend, F.; Ahlrichs, R. *Phys. Chem. Chem. Phys.* **2005**, *7*, 3297.
(41) van Lenthe, E.; Baerends, E. J.; Snijders, J. G. *J. Chem. Phys.* **1993**, *99*, 4597.
(42) Neese, F. *J. Chem. Phys.* **2001**, *115*, 11080.
(43) Neese, F. *J. Chem. Phys.* **2003**, *118*, 3939.
(44) Perdew, J. P.; Burke, K.; Ernzerhof, M. *Phys. Rev. Lett.* **1996**, *77*, 3865.
(45) van Lenthe, E.; Baerends, E. J.; Snijders, J. G. *J. Chem. Phys.* **1993**, *99*, 4597.
(46) van Lenthe, E.; Baerends, E. J.; Snijders, J. G. *J. Chem. Phys.* **1994**, *101*, 9783.
(47) Solomon, E. I. In *Comments in Inorganic Chemistry*; Sutin, N., Ed.; Gordon and Breach: New York, 1984; Vol. 3.
(48) Pick, F. M.; McGartol, M.; Bray, R. C. *Eur. J. Biochem.* **1971**, *18*, 65.
(49) Barber, M. J.; Bray, R. C.; Lowe, D. J.; Coughlan, M. P. *Biochem. J.* **1976**, *153*, 297.
(50) Mabbs, F. E.; Collison, D. *Electron Paramagnetic Resonance of d Transition Metal Compounds*; Elsevier: Amsterdam, The Netherlands, 1992.
(51) Nipales, N. S.; Westmoreland, T. D. *Inorg. Chem.* **1997**, *36*, 756.
(52) Drew, S. C.; Hill, J. P.; Lane, I.; Hanson, G. R.; Gable, R. W.; Young, C. G. *Inorg. Chem.* **2007**, *46*, 2373.
(53) Drew, S. C.; Young, C. G.; Hanson, G. R. *Inorg. Chem.* **2007**, *46*, 2388.
(54) Bridgeman, A. J.; Cavigliasso, G.; Ireland, L. R.; Rothery, J. *Dalton Trans.* **2001**, 2095.
(55) Kirk, M. L.; Shultz, D. A.; Habel-Rodriguez, D.; Schmidt, R. D.; Sullivan, U. *J. Phys. Chem. B* **2010**, *114*, 14712.
(56) McNaughton, R. L.; Helton, M. E.; Cosper, M. M.; Enemark, J. H.; Kirk, M. L. *Inorg. Chem.* **2004**, *43*, 1625.
(57) McNaughton, R. L.; Tipton, A. A.; Conry, R. R.; Kirk, M. L. *Inorg. Chem.* **2000**, *39*, 5697–5706.
(58) Peariso, K.; Helton, M. E.; Duesler, E. N.; Shadle, S. E.; Kirk, M. L. *Inorg. Chem.* **2007**, *46*, 1259.
(59) Reed, A. E.; Curtiss, L. A.; Weinhold, F. *Chem. Rev.* **1988**, *88*, 899.
(60) Wiberg, K. B. *Tetrahedron* **1968**, *24*, 1083.
(61) Doonan, C. J.; Rubie, N. D.; Peariso, K.; Harris, H. H.; Knottenbelt, S. Z.; George, G. N.; Young, C. G.; Kirk, M. L. *J. Am. Chem. Soc.* **2008**, *130*, 55.
(62) Westcott, B. L.; Gruhn, N. E.; Enemark, J. H. *J. Am. Chem. Soc.* **1998**, *120*, 3382.

(63) Inscore, F. E.; Knottenbelt, S. Z.; Rubie, N. D.; Joshi, H. K.; Kirk, M. L.; Enemark, J. H. *Inorg. Chem.* **2006**, *45*, 967.
(64) Kirk, M. L.; McNaughton, R. L.; Helton, M. E. *Prog. Inorg. Chem.* **2004**, *52*, 111.
(65) Alabugin, I. V.; Manoharan, M. *J. Phys. Chem. A* **2002**, *107*, 3363.
(66) Pross, A.; Shaik, S. S. *Acc. Chem. Res.* **1983**, *16*, 363.